A&A manuscript no.
(will be inserted by hand later)

Your thesaurus codes are:
07 (08.01.1; 08.02.2; 08.05.3; 08.06.3; 08.09.2 LB 3459; 08.12.2)

ASTRONOMY AND ASTROPHYSICS
February 16, 2000

NLTE spectral analysis of the sdOB primary of the eclipsing binary system LB 3459 (AA Dor)*

T. Rauch

Institut für Astronomie und Astrophysik, Universität Tübingen, Germany

Received 2 December 1999 / Accepted 9 February 2000

Abstract. We present a spectral analysis of the sdOB primary star of the binary system LB 3459 based on high-resolution high-S/N optical and UV spectra. The metal abundances are determined by means of state-of-the-art NLTE model atmospheres.

We determined $T_{\text{eff}} = 42$kK and $\log g = 5.2$ within very small error limits. The He (1/125 solar), C (1/265), N (1/33), O (1/12), and Si (1/5) abundances appear strongly depleted while that of Fe and Ni are roughly solar and Mg is strongly enriched by a factor of 6.

The spectroscopic distance to LB 3459 is $d = 396$ pc. The mass of the primary component of LB 3459 is $0.330\,\mathrm{M}_\odot$ derived from comparisons with theoretical models for sdO stars in the $\log T_{\text{eff}} - \log g$ plane. The mass of the secondary is then $0.066\,\mathrm{M}_\odot$ derived from the mass function. There remains some disagreement between the radius derived from $\log g$ and the above mass, and that derived from analysis of the radial-velocity curve and the eclipse curves. LB 3459 is a close binary system which had experienced a common envelope (CE) phase during its evolution. It fits in the "low mass case B" scenario of Iben & Livio (1993) and the secondary is a brown dwarf.

The spectroscopically determined rotational velocity of the primary is $v_{\text{rot}} = 34 \pm 10\,\text{km} \cdot \text{sec}^{-1}$. Thus even bound rotation ($v_{\text{rot}} = 45.7\,\text{km} \cdot \text{sec}^{-1}$) cannot be ruled out.

Key words: stars: abundances – stars: binaries: eclipsing – stars: evolution – stars: fundamental parameters – stars: individual: LB 3459 – stars: low-mass, brown dwarfs

1. Introduction

LB 3459 (HD 269696) is a very blue ($B-V = -0.27, U-B = -1.10$, Wesselink 1962) peculiar early-type foreground object ($m_{\text{V}} = 11.2$) of the Large Magellanic Cloud region (Feast et al.1960) with a variable spectrum.

Early studies of LB 3459 by Kilkenny et al. (1978, 1979, 1981) and Paczynski (1980) established that the system is composed of an sdO primary star and a low-mass degenerate dwarf star of low temperature.

The first spectral analysis of the sdO primary star of LB 3459 by means of NLTE model atmosphere techniques was performed by Kudritzki et al.(1982). They determined $T_{\text{eff}} = 40^{+3}_{-2}$kK, $\log g = 5.3 \pm 0.2$ (cgs), $n_{\text{He}}/n_{\text{H}} = 0.003^{+0.002}_{-0.001}$ (by number) which is extraordinary small, $M_1 = 0.3\,\mathrm{M}_\odot$, and $M_2 = 0.04\,\mathrm{M}_\odot$. This analysis was hampered by the lack of adequate numerical methods and computational capacity at that time, and thus only rudimental model atoms of hydrogen and helium could be considered (Kudritzki 1976).

Kudritzki et al.(1982) proposed diffusion to cause the He depletion in the photosphere of LB 3459. This was supported by an analysis of the carbon and silicon abundances by Lynas-Gray et al. (1984) using high-resolution IUE spectra. They found that these elements are depleted by factors of 100 and 10, respectively.

Based on the newly developed Accelerated Lambda Iteration (ALI) method (Werner & Husfeld 1985, Werner 1986) Rauch (1987) calculated new hydrogen NLTE models (lowest 15 H I levels treated in NLTE, all respective line transitions) in order to verify that the low $n_{\text{He}}/n_{\text{H}}$ ratio was not an artifact due to an error in the determination of T_{eff} (Heber et al. 1988). Rauch (1987) reproduced well the observations at $T_{\text{eff}} = 40$kK and excluded definitely $T_{\text{eff}} > 50$ kK. He concluded that the $n_{\text{He}}/n_{\text{H}}$ ratio is even lower (at least a tenth) than found by Kudritzki et al.(1982, see Tab. 4).

LB 3459 has been classified to be a post-common envelope (CE) sdOB + MS binary (de Kool & Ritter 1993). Binaries containing an sdOB star are rosetta stones for the understanding of CE evolution since the lifetime of this component is much shorter than the orbital evolution time scale of the binary (de Kool & Ritter 1993). The CE evolution is discussed in detail e.g. by Iben & Livio (1993).

Hilditch et al. (1996, hereafter HHH) have recently analyzed the light and radial-velocity curves of LB 3459 and determined its orbital parameters precisely. Since a wide range for the primary mass ($0.14\mathrm{M}_\odot \lesssim M_1 \lesssim 0.46\mathrm{M}_\odot$) is possible within the error limits of $\log g$ given by Kudritzki et al. (1982), and hence, even a very low secondary mass of $M_2 = 0.02\mathrm{M}_\odot$ appears

Send offprint requests to: T. Rauch

* Based on observations collected at the European Southern Observatory, La Silla, Chile (proposals 55.D-0319, 56.C-0165) and on data retrieved from the International Ultraviolet Explorer (IUE) Final Archive

Correspondence to: rauch@astro.uni-tuebingen.de

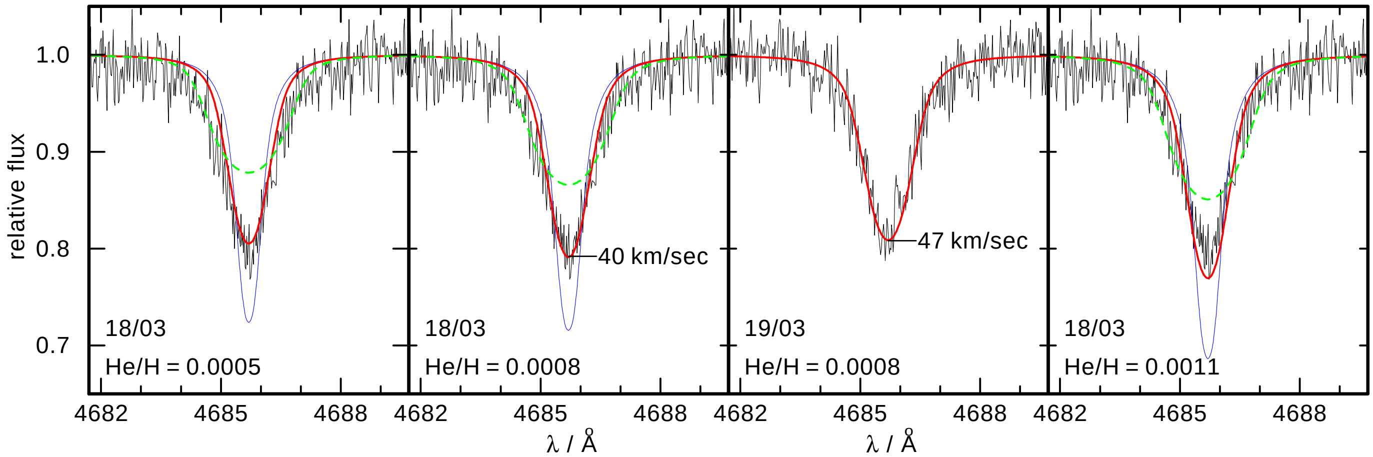

Fig. 1. Comparison of theoretical He II λ 4686Å line profiles to the CES spectra of the 18/03 and 19/03 (Tab. 1). The models are calculated with $T_{\rm eff}$ = 42kK, log g = 5.2, and He/H = 0.0007, 0.0010, 0.0013. The theoretical profiles are convolved with rotational profiles with $v_{\rm rot}$ = 8 (thin), 40 (thick), and 80km $\cdot$ sec^{-1} (dashed) and with a Gaussian (FWHM = 0.1 Å). In the case of the 19/03 spectrum, 47km $\cdot$ sec^{-1} is used

Table 1. Observation log of the optical spectra of LB 3459 taken at ESO

telescope	instrument	date	exposure time / sec	wavelength range / Å	resolution / Å	observer
3.6m	CASPEC	11.10.85	3600	3927 - 4940	0.25	Heber
3.6m	CASPEC	11.10.85	3600	5750 - 6803	0.30	Heber
NTT	EMMI	08.04.95	600	3785 - 4710	2.65	Rauch
NTT	EMMI	10.04.95	700	4240 - 5100	2.95	Rauch
CAT	CES	16.03.96	3600	H α	0.12	Rauch
CAT	CES	17.03.96	3600	H α	0.12	Rauch
CAT	CES	18.03.96	3600	He II λ 4686Å	0.10	Rauch
CAT	CES	19.03.96	3600	He II λ 4686Å	0.10	Rauch

likely, HHH illustratively assumed that the primary has a mass of $M_1 = 0.5\,\mathrm{M}_\odot$ and arrived at a mass of $M_2 = 0.086\,\mathrm{M}_\odot$ for the secondary. Since they have presented a well defined orbital solution for LB 3459, their M_2 is as good as their M_1 assumption. Thus, the secondary might be a brown dwarf with a lower mass as well. HHH concluded that a new determination of log g is urgently required in order to solve this problem.

To make progress, we have collected new spectra with ESO telescopes at La Silla (Tab. 1) and have now a complete coverage of the optical wavelength range. Together with IUE spectra which are available in the Final Archive, we determine the photospheric properties of LB 3459 within small error ranges (Sect. 3.2). The metal abundances (C, N, O, Mg, Si, Fe, and Ni) are determined by means of state-of-the-art NLTE model atmosphere techniques (Sect. 3.4). The masses of both, primary and secondary, are determined from comparison with evolutionary tracks and from the mass function of LB 3459 (Sect. 3.4.8).

2. Observations

Optical spectra of LB 3459 were obtained during several observation campaigns in the last years. In Tab. 1 we summarize these observations. The given resolution is measured from the He-Ar and Th-Ar comparison spectra.

Table 2. IUE spectra of LB 3459 retrieved from the Final Archive

image	resolution	date	exposure time sec	shift Å
SWP 03729	high	28.12.78	10680	−0.08
SWP 04887	low	8.04.79	437	
SWP 17821	high	31.12.82	6000	−0.18
SWP 17822	high	31.12.82	6000	+0.05

We retrieved the three available high-resolution SWP spectra of LB 3459 from the IUE Final Archive (Tab. 2). Since LB 3459 is a binary, we used H I λ 1215Å, He II λ 1640Å, C IV $\lambda\lambda$ 1548, 1550Å, N IV λ 1718Å, N V $\lambda\lambda$ 1238, 1242 Å, and Si IV $\lambda\lambda$ 1393, 1402Å in order to determine the average shifts from their rest wavelengths (Tab. 2). All these lines show the same deviations and are thus clearly of photospheric origin while e.g. Si III λ 1206Å (Fig. 5) appears at its rest wavelength in all spectra and hence, is dominated by interstellar absorption. The spectra are shifted then by these amounts and co-added (equally-weighted due to their similar S/N ratio). The influence of the orbital motion of LB 3459 is discussed in (Sect. 3.1).

3. NLTE analysis

Since the spectral analysis presented by Kudritzki et al. (1982) and Heber et al. (1988) our (plane-parallel, hydrostatic) NLTE model atmospheres have been significantly improved, e.g. by the consideration of level dissolution following the Hummer-Mihalas (1988) occupation probability formalism for H I and He II (Hubeny et al. 1994, Werner 1996). The employed model atoms are much more detailed (Rauch 1997) and we consider additionally Stark line broadening for the H I and He II $n = 1, 2, 3$ series (Werner 1996). The line opacities are considered up to a distance to the line center of 3 000 Doppler widths. In the following we describe our new spectral analysis.

3.1. The rotational velocity of LB 3459

Since the orbital period of LB 3459 is short ($P = 0.26$d), both, the rotation of the primary and its orbital motion during the relatively long exposure times (Table 1, 2) will contribute to the line broadening. HHH have determined a velocity amplitude $K_1 = 40.8\mathrm{km}\cdot\mathrm{sec}^{-1}$ for the primary of LB 3459. In Fig. 2 we show the observations in relation to the orbital phase ϕ as defined by HHH.

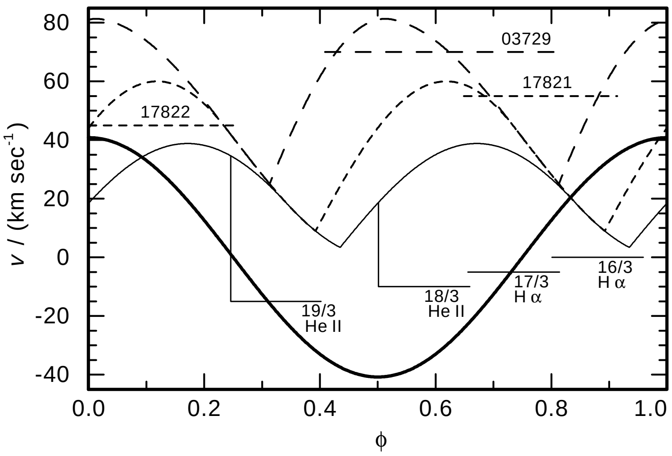

Fig. 2. The radial velocity curve of LB 3459. The phase is given with respect to the maximum positive velocity. The CES observations (Tab. 1) and the IUE SWP exposures (Tab. 2) are indicated. The thin curve indicates the maximum velocity coverage during an exposure of 3 600 sec (small dashes: 6 000 sec, long dashes: 10 680 sec, respectively) for a given start phase

For a precise determination we use our CES spectra (Tab. 1) of He II λ 4686Å which have the best resolution and (at least the 18/03 spectrum) a relatively small contribution from the orbital motion. In Fig. 1 we show fits of theoretical profiles to the observation with $T_{\mathrm{eff}} = 42$kK, $\log g = 5.2$, different He/H abundance ratios, and different v_{rot}. Obviously, the observed line profiles in the 18/03 and 19/03 spectrum are slightly different due to the different orbital phase during the observation (Fig. 2). $v_{\mathrm{rot}} = 40$ and $47\mathrm{km}\cdot\mathrm{sec}^{-1}$ are necessary in order to achieve a sufficient fit, respectively. From Fig. 2 we derive velocity coverages of 18.7 and $34.6\mathrm{km}\cdot\mathrm{sec}^{-1}$ during the 18/03 and 19/03 observation, respectively. With these values and the rough approximation $v^2_{\mathrm{rot}} = v^2_{\mathrm{total}} - v^2_{\mathrm{coverage}}$, $v_{\mathrm{rot}} = 35.6$ and $31.8\mathrm{km}\cdot\mathrm{sec}^{-1}$ ($\pm 10\mathrm{km}\cdot\mathrm{sec}^{-1}$) is calculated for the primary. At the given quality of the spectra, these values appear to be in good agreement. From their mean of $v_{\mathrm{rot}} = 33.7\mathrm{km}\cdot\mathrm{sec}^{-1}$ and the minimum value of the velocity difference of $v_{\mathrm{d}} = 3.4\mathrm{km}\cdot\mathrm{sec}^{-1}$ for a 3 600 sec exposure (Fig. 2), we can estimate a minimum of $v_{\mathrm{total}} = 37.1\mathrm{km}\cdot\mathrm{sec}^{-1}$ which is the best case. However, the exact starting time of the CASPEC observations (Tab. 1) is not known and we do not expect best conditions. Thus, we adopt $v_{\mathrm{rot}} = 45\mathrm{km}\cdot\mathrm{sec}^{-1}$ for our further analysis. This value appears suitable for the IUE spectra SWP 17821 and 17822 as well (Fig. 2).

3.2. Effective temperature and surface gravity

Firstly we carried out test calculations with $T_{\mathrm{eff}} = 40$kK and $\log g = 5.3$ (Kudritzki et al. 1982) and found that $n_{\mathrm{He}}/n_{\mathrm{H}} = 0.0010$ (by number) fits the observation (around He II λ 4686Å) sufficiently well. With this preliminary helium abundance (Sect. 3.4.1), we calculated a grid of H+He models (T_{eff} = 30 000 – 47 000 K in 250 K steps, $\log g$= 4.50 – 5.90 (cgs) in steps of 0.05 dex). From these models, synthetic spectra were calculated using the line-broadening tables calculated by Lemke (1997) and by Schöning & Butler (1989), based upon the VCS theory (Vidal et al. 1973)

In a coarse approach, the effective temperature T_{eff} and the surface gravity g were determined by fitting the synthetic spectra which are convolved firstly with a rotational profile ($v_{\mathrm{rot}} = 45\,\mathrm{km}\cdot\mathrm{sec}^{-1}$) and then with a Gaussian with a FWHM according to the spectral resolution (Tab. 1) to the normalized EMMI and CASPEC spectra (Tab. 1). A χ^2 test (cf. Bevington & Robinson 1992) was performed and the results are $T_{\mathrm{eff}} = 42.25$kK and $\log g = 5.35$, and $T_{\mathrm{eff}} = 41$kK and $\log g = 5.18$, respectively. Although these agree within their error limits, it turned out that it is impossible to achieve a perfect simultaneous fit of H α – H ϵ at these values: We are running into a mild form of the well-known Balmer-line problem (Napiwotzki & Rauch 1994). This indicates that the photospheric temperature structure of LB 3459 is not well modeled due to the neglected metal-line blanketing in our H+He models (Werner 1996, Fig. 3).

We performed a χ^2 test, this time in order to fit H α – H ϵ individually. In the CASPEC spectrum, the observed profiles of H α and H β (Fig. 18) appear asymmetric (most likely due to problems during the data reduction) and thus, we achieve different results if we split the region in two parts, bluewards and redwards of the line centers. Hence these lines are not useful. The results of H γ – H ϵ are shown in Fig. 4. These three lines (both, CASPEC and EMMI spectrum) indicate an average surface gravity of $\log g = 5.21$ within a very small error range.Thus, we finally adopt this value.

The derived T_{eff} increases towards the higher series members which, again, is most likely due to the neglect of metal opacities and the resulting Balmer line problem (Werner 1986).

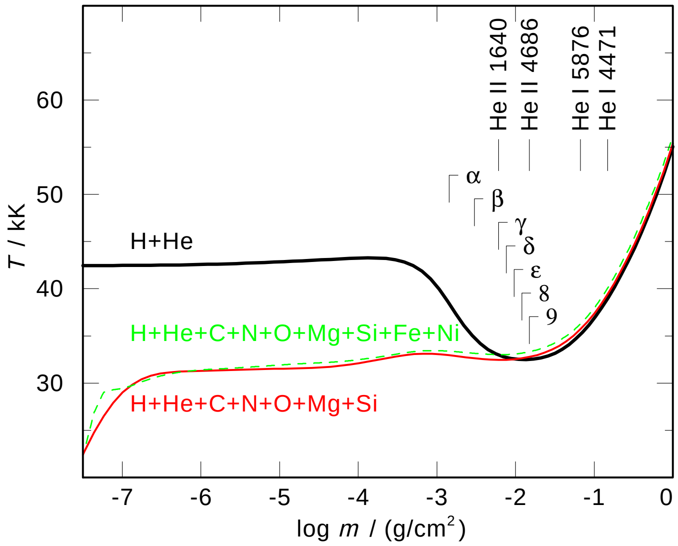

Fig. 3. Formation depths of the line cores of H α – H 9, He I $\lambda\lambda$ 4471, 5876Å, and He II $\lambda\lambda$ 1640, 4686Å. In the model ($T_{\rm eff} = 42$kK, $\log g = 5.2$) which accounts for metal-line blanketing of C+N+O+Mg+Si, the temperature is much lower at the formation depths of the lower member of the H I Balmer series, e.g. $\approx$ 20 % at H α. The dotted line shows the temperature of our final model with Fe+Ni in addition. m is the column mass in the stellar atmosphere. Model parameters see Tab. 4

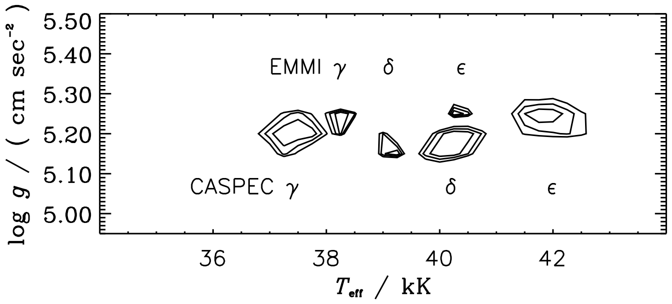

Fig. 4. Results of χ^2 tests performed in order to determine $T_{\rm eff}$ and $\log g$. $\gamma - \epsilon$ denote the results if we use -40 Å $\leq \lambda - \lambda_0 \leq +40$ Å of the CASPEC and EMMI spectra for the Balmer lines, respectively. The contours given indicate the formal 1 σ, 2 σ, and 3 σ error ranges

Since the higher members of the Balmer series form deeper inside the atmosphere (Fig. 3) where the influence of metal-line blanketing on the photospheric structure is smaller, $T_{\rm eff}$ derived from those is more reliable. The formation depths of the Balmer lines (Fig. 3) indicate that H ϵ forms deep enough in the atmosphere to be suited for a reliable determination of $T_{\rm eff}$. From this line (CASPEC spectrum) we derive $T_{\rm eff} = 42$kK. However, for a more precise determination we evaluate the ionization equilibrium of He I / He II which is a sensitive indicator of $T_{\rm eff}$ (Fig. 7). Moreover, the He lines form deeper in the atmosphere than H α and H β (Fig. 3) and thus, are more reliable than those. For $T_{\rm eff} <$ 42 kK He I $\lambda\lambda$ 4471, 5876Å appear too strong. At $T_{\rm eff} = 42$kK the theoretical He I λ 5876Å line profile fits well the observation. Within this $T_{\rm eff}$ range, He II $\lambda\lambda$ 1640, 4686Å show only very small changes in the inner line cores. We preliminarily adopt this value which will be verified in the following by the examination of the ionization equilibria of other elements which are identified in the spectrum of LB 3459.

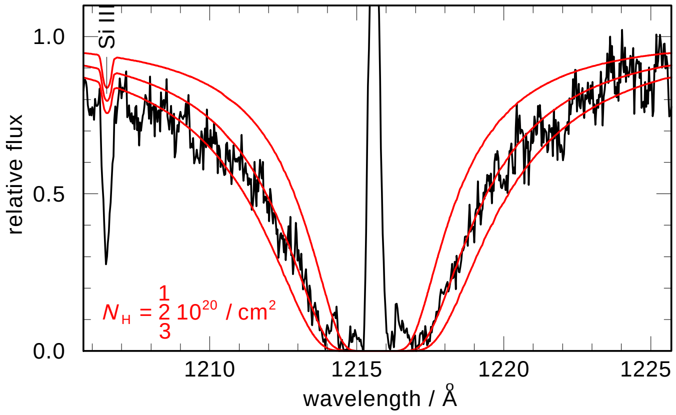

Fig. 5. Theoretical line profile of H I Ly α from our final H+He+C+N+O+Mg+Si model (Tab. 4) compared with the IUE spectrum of LB 3459. Interstellar absorption has been considered with H I column densities of $1 \cdot 10^{20}$, $2 \cdot 10^{20}$, and $3 \cdot 10^{20}/\mathrm{cm}^2$. Note that the photospheric Si III λ 1206Å is blended by interstellar absorption (Sect. 2)

3.3. Interstellar absorption

We have used the co-added IUE spectrum of LB 3459 in order to determine the neutral hydrogen column density from the Ly α interstellar absorption. An inspection of the observation shows that the background correction around Ly α is not perfect. Thus, we subtracted the estimated remaining background and normalized the spectrum. A theoretical spectrum with $n_{\rm H} = 2 \cdot 10^{20}/\mathrm{cm}^2$ fits well the observation (Fig. 5). A color excess $E_{\rm B-V} = 0.0526$ is calculated using the formula given by Groenewegen & Lamers (1989).

3.4. Photospheric abundance ratios

In the spectrum of LB 3459 we have identified H, He, C, N, O, Mg, and Si lines. We will now determine the photospheric abundance ratios of these elements. Therefore we calculated new models and considered element by element in addition, i.e. the He/H ratio is determined from H+He models, the C/H ratio from H+He+C models, and so on. In each case, we checked the influence of the newly considered element on the previous results.

3.4.1. He/H

We calculated H+He models ($T_{\rm eff} = 42$kK, $\log g = 5.2$) with different abundance ratios and performed a χ^2 test using our optical spectra (Tab. 1) and He II λ 4686Å. The result is shown in Fig. 6.

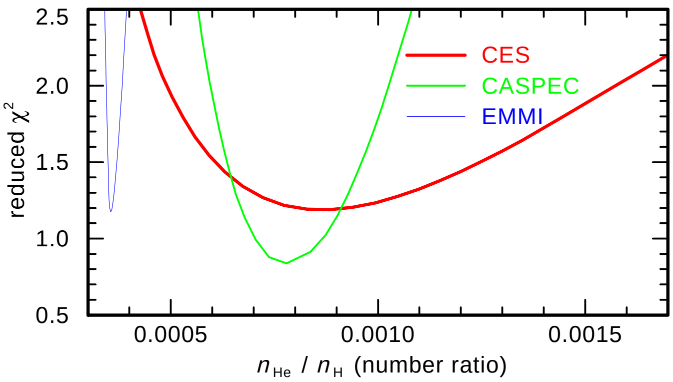

Fig. 6. Reduced χ^2 values of our fitting procedure to the observed He II λ 4686Å line profile. From the CES, CASPEC, and EMMI spectra (Tab. 1), we derive $n_{\mathrm{He}}/n_{\mathrm{H}}$ values of 0.0009, 0.0008, and 0.0004, respectively. However, since the resolution of the EMMI spectrum (Tab. 1) is comparable to the line width of He II λ 4686Å, this result is less reliable

Due to the much better resolution of the CES and CASPEC spectra (Tab. 1) and thus a larger error range for the EMMI result, we have finally adopted $n_{\mathrm{He}}/n_{\mathrm{H}} = 0.0008 \pm 0.0002$.

The fit of He I $\lambda\lambda$ 4471, 5876Å and He II $\lambda\lambda$ 1640, 4686Å at $T_{\mathrm{eff}} \lesssim 42$ kK shows both theoretical He I lines too strong while He II λ 4686Å appears too shallow. Since the ionization equilibrium is a very sensitive indicator of T_{eff}, T_{eff} has to be higher: At $T_{\mathrm{eff}} = 42$kK we achieve good agreement with the observation (Fig. 7).

3.4.2. C/H

In order to determine the C/H abundance ratio, we calculated models with $T_{\mathrm{eff}} = 42$kK, $\log g = 5.2$, $n_{\mathrm{He}}/n_{\mathrm{H}} = 0.0010$, and carbon in addition. We used the most prominent carbon lines in the co-added IUE spectrum, the C III $\lambda\lambda$ 1175Å complex, and the C IV $\lambda\lambda$ 1548, 1550Å resonance doublet. The best fit is achieved with $n_{\mathrm{C}}/n_{\mathrm{H}} = 1.5 \cdot 10^{-6}$ (Fig. 8).

3.4.3. N/H

The N/H abundance ratio is determined analogously to the C/H ratio (Sect. 3.4.2). We used the model parameters from that analysis and added nitrogen. The best fit to lines from the ionization stages N III – N V is achieved at $n_{\mathrm{N}}/n_{\mathrm{H}} = 3 \cdot 10^{-6}$ (Fig. 9).

3.4.4. O/H

In the UV spectrum, O IV $\lambda\lambda$ 1338, 1342, 1343Å and O V λ 1371Å are identified. We used these lines to determine the O/H ratio (Fig. 10). A sufficient fit is achieved at $n_{\mathrm{O}}/n_{\mathrm{H}} = 6.4 \cdot 10^{-5}$ The available IUE spectra in the O V λ 1371Å wavelength region show a broad absorption trough. However, the O V line is clearly present, and is reproduced well if it is normalized to the local continuum (Fig. 10). The synthetic spectrum of our final

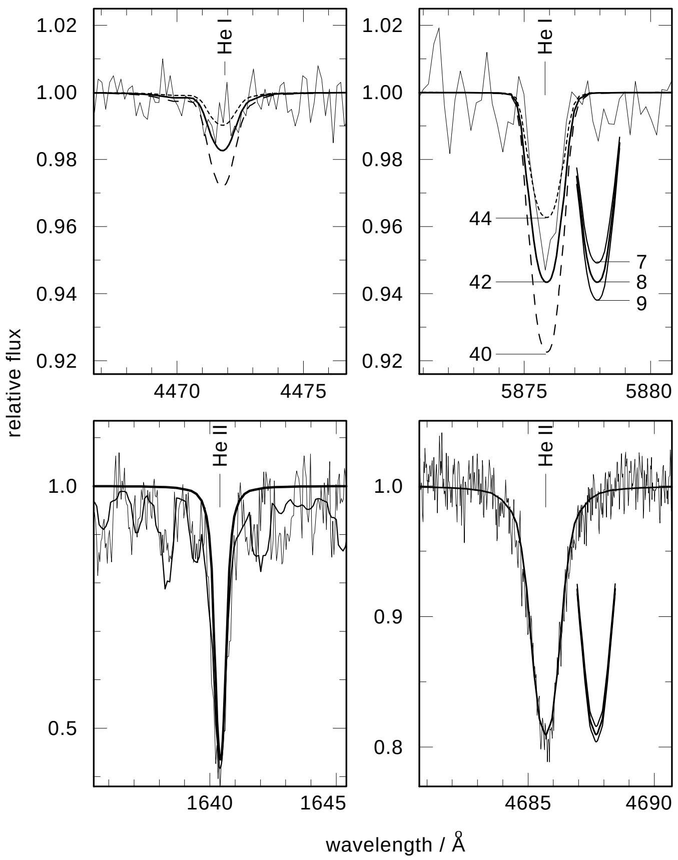

Fig. 7. Fit to the line profiles of He I $\lambda\lambda$ 4471, 5876Å and of He II $\lambda\lambda$ 1640, 4686Å at $T_{\mathrm{eff}} = 40$kK (dashed), $T_{\mathrm{eff}} = 42$kK (fully drawn), $T_{\mathrm{eff}} = 44$kK (dotted), $\log g = 5.2$, and $n_{\mathrm{He}}/n_{\mathrm{H}} = 0.0008$ compared with the CASPEC (upper panel), co-added IUE (lower panel left, cf. Tab. 2) and CES spectrum (lower panel, right) of LB 3459. In the case of He I λ 5876Å and He II λ 4686Å, we show also the abundance dependency of their line cores ($n_{\mathrm{He}}/n_{\mathrm{H}} = 0.0007, 0.0008, 0.0009$). For clarity, these profiles are shifted by +2Å. In the case of He II λ 1640Å, the thin line shows the normalized flux of our final H+He+C+N+O+Mg+Si+Fe+Ni model (Tab. 4). Note the different flux scales

H+He+C+N+O+Mg+Si+Fe+Ni (Fig. 10) shows that the continuum around O V λ 1371Å is dominated by Fe and Ni lines.

3.4.5. Mg/H

Unfortunately, neither Mg II nor Mg III (dominant ionization stage in the line forming region) lines are unambiguously identified in the IUE spectrum due to its S/N ratio and the bulk of metal lines which are present therein. Thus, the Mg/H ratio has to be determined from Mg II λ 4481Å alone (Fig. 11). At a surprisingly high ratio of $n_{\mathrm{Mg}}/n_{\mathrm{H}} = 1.9 \cdot 10^{-4}$, which is six times the solar ratio, we achieve a sufficient fit to the observation.

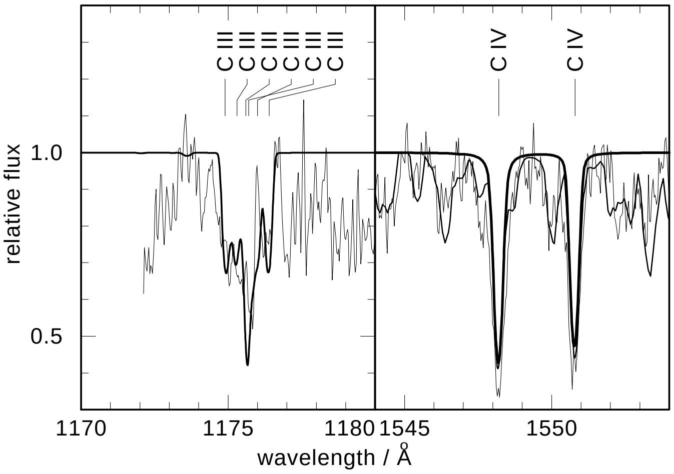

Fig. 8. Fit to the line profiles of C III $\lambda\lambda$ 1175Å and C IV $\lambda\lambda$ 1548, 1550Å (model parameters see Tab. 4) compared with the IUE (SWP 03729) spectrum of LB 3459. In the right panel, the thin line shows the normalized flux of our final H+He+C+N+O+Mg+Si+Fe+Ni model (Tab. 4). The observation is smoothed using a Savitzky-Golay filter (Press et al. 1992)

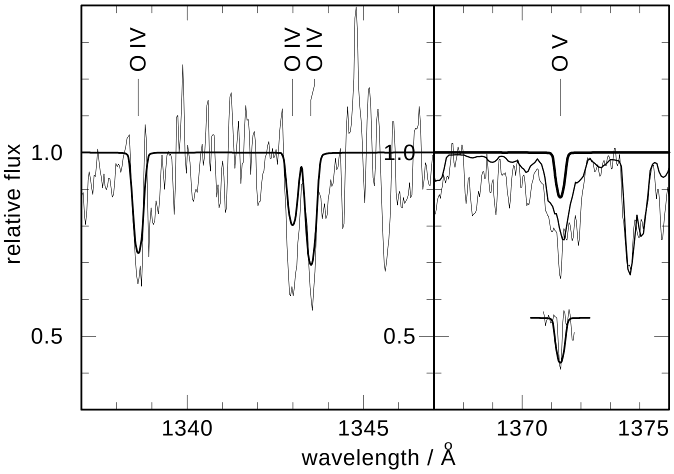

Fig. 10. Fit to the line profiles of O IV $\lambda\lambda$ 1338, 1342, 1343Å (left) and O V λ 1371Å (right) (H+He+C+N+O model parameters see Tab. 4) compared with the spectrum (SWP 17821 only) of LB 3459. At the bottom of the right panel, the theoretical spectrum is normalized to the local continuum: O V λ 1371Å matches the local feature. The thin line (right) shows the spectrum of our final model with Mg+Si+Fe+Ni in addition which improves the overall fit to the observation. However, no perfect fit of the region around O V λ 1371Å is achieved

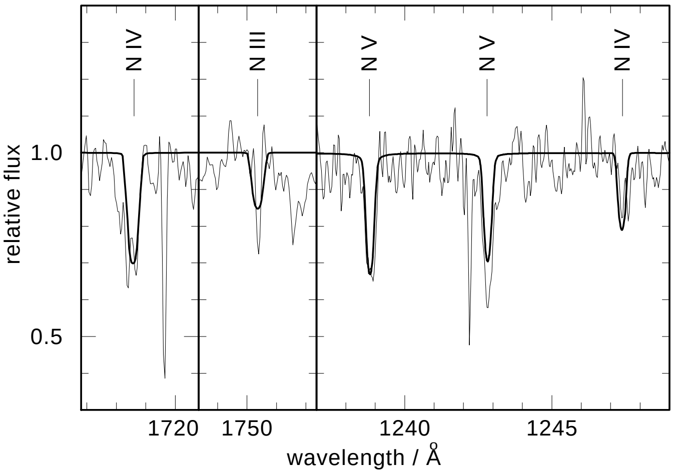

Fig. 9. Fit to the line profiles of N III λ 1750Å, N IV λ 1718Å, and N V $\lambda\lambda$ 1238, 1248Å (model parameters see Tab. 4) compared with the spectrum of LB 3459

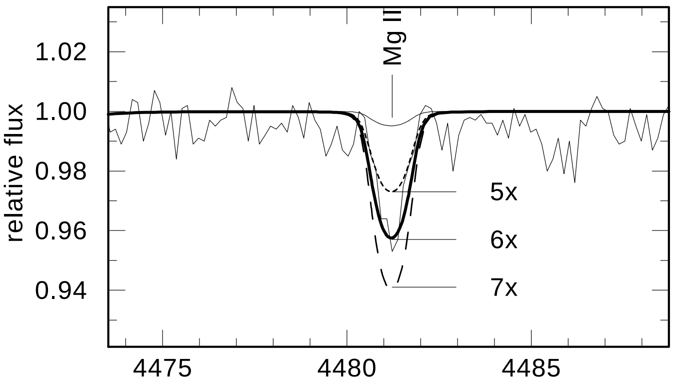

Fig. 11. Fit to the line profile of Mg II λ 4482Å at different Mg/H ratios: solar (thin line), 5 (dotted), 6 (thick line), and 7 (dashed) times solar (other model parameters see Tab. 4) compared with the CASPEC spectrum of LB 3459

3.4.6. Si/H

Unfortunately, Si III λ 1206Å (Fig. 5) seems to be contaminated by an interstellar component (Sect. 2) and we can use the Si IV $\lambda\lambda$ 1393, 1402Å resonance doublet for this analysis, only. The best fit is achieved at $n_{\rm Si}/n_{\rm H} = 8 \cdot 10^{-6}$ (Fig. 12). At this ratio, the Si lines which are identified in the optical spectrum are well reproduced, e.g. Si IV $\lambda\lambda$ 4088, 4116Å which are shown in Fig. 18.

3.4.7. Fe and Ni

Helium and the light metals C, N, O, and Si appear underabundant in the photosphere of LB 3459 compared to solar values while Mg is enriched. In a last step we determine the Fe and Ni abundances. We calculated a final model (parameters see Tab. 4) with Fe and Ni in addition. Their opacities are considered following Deetjen et al. (1999). The statistics of our model atoms for these calculations are summarized in Tab. 3.

We used a fixed (solar) Fe/Ni ratio and compared theoretical spectra with different Fe/H ratios with a low-resolution IUE spectrum (Fig. 13) which is well suited for this purpose. At the solar Fe/H ratio, the overall agreement with the spectral shape is much improved compared to a "pure" H+He+C+N+O+Mg+Si model. Fe/H ratios which are higher or lower by 0.5 dex provide worse results.

The comparison to the available high-resolution IUE spectra of LB 3459 allows to identify the strongest Fe and Ni lines (Fig. 14, see also Figs. 7, 8, and 10). From the fit to the observation, a Ni/Fe ratio much different from solar can be excluded.

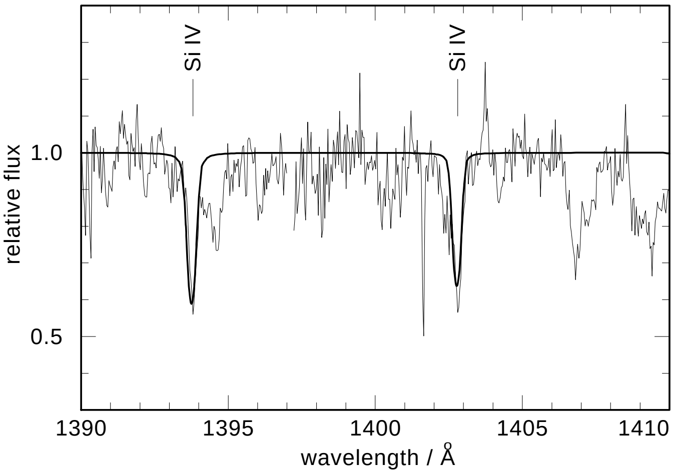

Fig. 12. Fit to the line profiles of Si IV $\lambda\lambda$ 1393, 1402Å (model parameters see Tab. 4) compared with the IUE spectrum of LB 3459. The strong absorption features which are not reproduced by this model are Fe and Ni lines (Fig. 14)

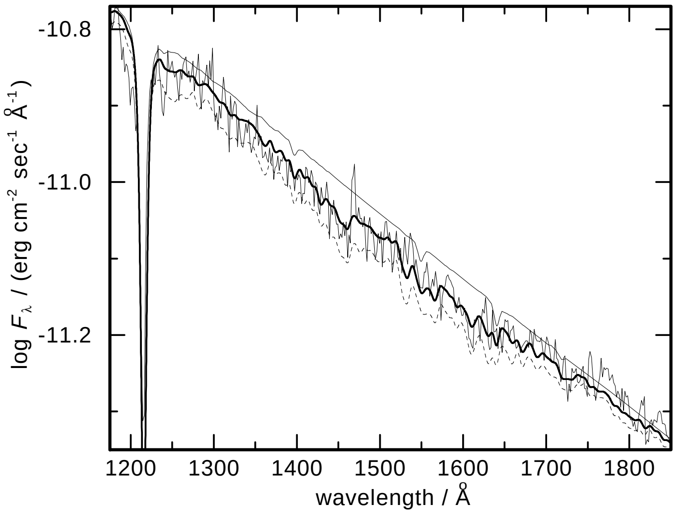

Fig. 13. Synthetic spectra of H+He+C+N+O+Mg+Si+Fe+Ni models with Fe/H = 0 (thin line), $3.2 \cdot 10^{-5}$ (thick line, $\approx$ solar value), and $2.56 \cdot 10^{-4}$ (dotted) compared with the UV spectrum (IUE SWP 04887, selected because it has the longest exposure time of 437 sec of the available low resolution spectra) of LB 3459. The three synthetic spectra are scaled by $6.46 \cdot 10^{-30}$ in order to match the observed flux level at 1700 Å with the Fe/H = 0 spectrum. Note that the flux from the model with eight times solar abundance is obviously too low. The theoretical flux is reddened according to our result. Parameters see Tab. 4

The comparison suggests that Ni might be mildly overabundant. However, the low S/N ratio and the high rotational velocity prevent a more precise analysis.

3.4.8. Mass, radius, and luminosity

The mass and the luminosity of the primary component of LB 3459 is determined by comparison with recently presented models departing from the first giant branch prior to core helium ignition and evolving into low-mass white dwarfs (Driebe et al. 1998). We derive $M_1 = 0.330 \pm 0.006\,\mathrm{M}_\odot$ (Fig. 15) and $L = 170 \pm 6\mathrm{L}_\odot$. The mass is 10% higher than determined by Kudritzki et al. (1982), who assumed an upper limit of $M_1 \leq 0.3\,\mathrm{M}_\odot$.
The radius of the primary can be calculated using

$$R_1 = \sqrt{\frac{G \cdot M_1}{g}} \qquad (1)$$

We calculate $R_1 = 0.236^{+0.031}_{-0.025}\mathrm{R}_\odot$.

Table 3. Statistics of the model atoms used for the calculation of final model of LB 3459. The notation is: NLTE = levels treated in NLTE, LTE = LTE levels, RBB = radiative bound-bound transitions. In the case of Fe and Ni, $\mathrm{NLTE_{st}}$ and $\mathrm{RBB_{st}}$ denote individual levels and transitions used in the statistical NLTE line-blanketing approach

atom	ion	NLTE	$\mathrm{NLTE_{st}}$	LTE	RBB	$\mathrm{RBB_{st}}$
H	I	16		0	120	
	II	1		-	-	
He	I	37		7	98	
	II	14		18	78	
	III	1		-	-	
C	III	13		71	19	
	IV	18		5	59	
	V	1		0	0	
N	III	1		0	0	
	IV	34		156	114	
	V	14		13	29	
	VI	1		0	0	
O	II	2		3	0	
	III	19		35	33	
	IV	11		58	19	
	V	5		7	3	
	VI	1		0	0	
Mg	I	5		1	3	
	II	14		19	34	
	III	15		20	20	
	IV	1		0	0	
Si	III	6		6	4	
	IV	16		7	44	
	V	4		12	2	
	VI	1		0	0	
Fe	IV	7	6 472	0	25	1 027 793
	V	7	6 179	0	25	793 718
	VI	8	3 137	0	33	340 132
	VII	9	1 195	0	39	86 504
	VIII	7	310	0	27	8 724
	IX	1		0	0	0
Ni	IV	7	5 514	0	25	949 506
	V	7	5 960	0	22	1 006 189
	VI	7	9 988	0	22	1 110 584
	VII	7	6 686	0	28	68 835
	VIII	7	3 600	0	27	553 549
	IX	1		0	0	0
	total	326	49 041	438	952	5 945 534

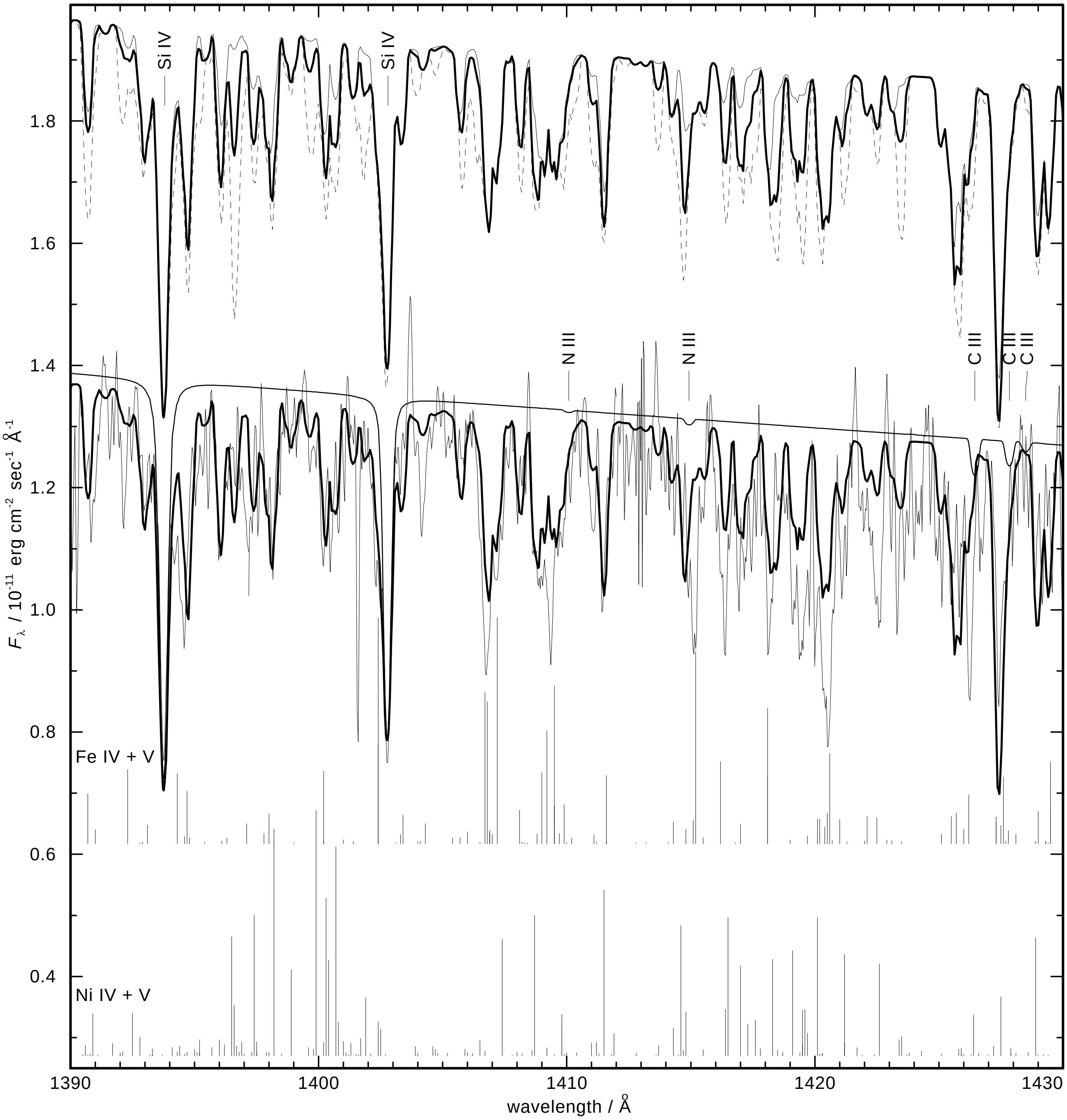

Fig. 14. Synthetic spectra of H+He+C+N+O+Mg+Si (thin line, in the middle) and H+He+C+N+O+Mg+Si+Fe+Ni models (parameters see Tab. 4) with Fe/Ni = 2 (dashed), 20 (thick line, solar ratio), and 200 (thin line) compared with a section of the IUE spectrum of LB 3459 (smoothed with a Savitzky-Golay filter, cf. Press et al. 1992). At solar Fe/H and Ni/H ratios, the observation is well matched. The Ni lines around $\lambda = 1420$Å might suggest a Fe/Ni ratio lower than solar. For clarity, three synthetic spectra with different Fe/Ni ratio are artificially shifted to the top. At the bottom, $\log gf$ values of Fe IV, Fe V, Ni IV, and Ni V are indicated (1 cm = $\log gf = 1$) as a hint for line identification

The mass of the secondary is calculated from the mass function given by HHH:

$$f(m) = \frac{M_2^3 \sin^3 i}{(M_1 + M_2)^2} = 0.00184 \pm 0.00009 \mathrm{M}_\odot \qquad (2)$$

($i = 90°$, Sect. 1). The solution is shown in Fig. 16. The mass of the secondary is $M_2 = 0.066 \pm 0.002\,\mathrm{M}_\odot$. This value is almost twice the value determined by Kudritzki et al. (1982).

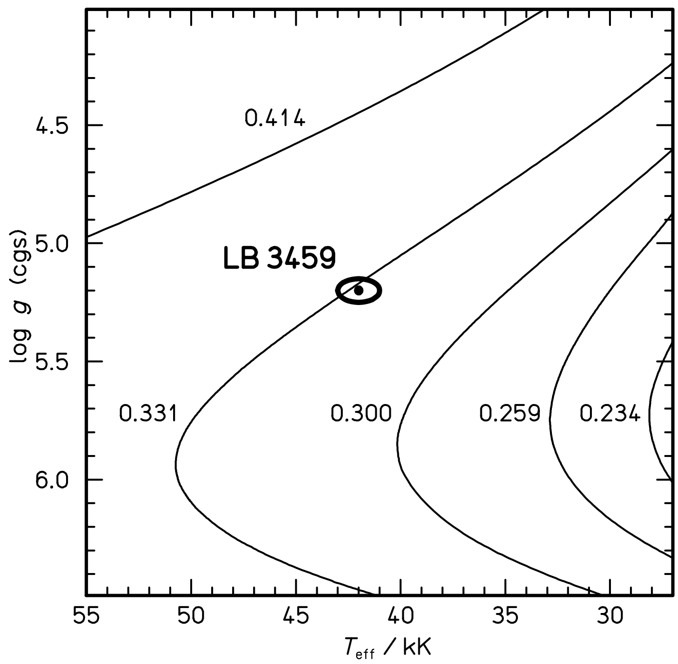

Fig. 15. Position of the primary component of LB 3459 in the $T_{\rm eff}$ - $\log g$ plane compared with theoretical evolutionary tracks of post-RGB stars (Driebe et al. 1998). The ellipse represents the derived errors in $T_{\rm eff}$ and $\log g$ (Tab. 4). The tracks are labeled with the respective stellar masses (in $M_{\odot}$)

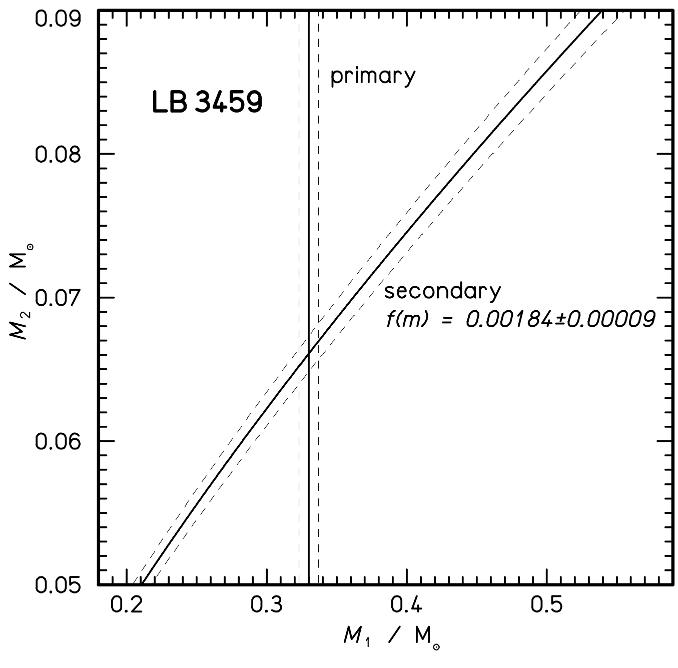

Fig. 16. Determination of the secondary's mass. From the mass function (Eq. 2) and $M_1 = 0.330\,M_{\odot}$, we derive $M_2 = 0.066\,M_{\odot}$

In order to compare our results with those from the analyses of the light curve and orbital parameters, we adopt $i = 90°$, $e = 0$, and $K_1 = 40.8\mathrm{km}\cdot\mathrm{sec}^{-1}$ the primary orbit is $a_1 = 0.21\mathrm{R}_{\odot}$. The separation $a = a_1 + a_2$ of the two components can be calculated using $a_1 M_1 = a_2 M_2$. Kilkenny et al. 1979 have given the relative radii: $r_1 = 0.138a$ and $r_2 = 0.079a$. In Fig. 17 the comparison is shown.

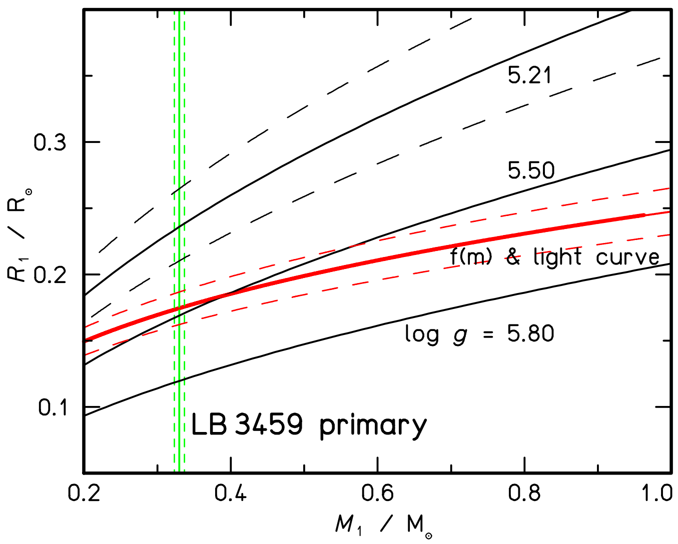

Fig. 17. Mass-radius relation for the primary of LB 3459. Obviously, the solution from f(m) & light curve does not intersect with our result ($\log g = 5.21$) and the mass value determined from comparison to evolutionary models (Fig. 15). The dashed lines indicate the error ranges

The results of our analysis are not in agreement with the solution of $f(m)$ & light curve analysis. The reason for this is unclear. A surface gravity $\log g \approx 5.5$ which is necessary for a fit at around $M_1 = 0.33\mathrm{R}_{\odot}$ can be excluded from the line profile fits to the available spectra. Only less strict (statistical) error ranges in both cases could provide a marginal agreement. We conclude that new spectra are necessary which are optimized in the view of orbital motion. This could definitely improve the spectral analysis.

3.5. Distance

Kudritzki et al. (1982) determined the distance $d = 280 \pm 100\,\mathrm{pc}$ of LB 3459 from its radius and the flux normalization.

From our final model, we can determine the spectroscopic distance of LB 3459 using the flux calibration of Heber et al. (1984):

$$f_{\rm V} = 3.58 \cdot 10^{-9} \cdot 10^{-0.4 m_{\rm V_0}} \mathrm{erg\,cm^{-2}\,sec^{-1}\,\AA^{-1}} \qquad (3)$$

with $m_{\rm V_0} = m_{\rm V} - 2.175c$, $c = 1.47 E_{\rm B-V} = 0.0773$ (Fig. 3.3), $m_{\rm V} = 11.2$ and $M = 0.330\mathrm{M}_{\odot}$, the distance is derived from

$$d = 7.11 \cdot 10^4 \sqrt{H_\nu \cdot M \cdot 10^{0.4 m_{\rm V_0} - \log g}}\ \mathrm{pc}\,. \qquad (4)$$

With the Eddington flux at $\lambda_{\rm eff} = 5454\text{Å}$ our final model atmosphere $H_\nu = 5.89 \cdot 10^{-4} \mathrm{erg\,cm^{-2}\,sec^{-1}\,Hz^{-1}}$ we derive a distance of $d = 396^{+50}_{-54}\,\mathrm{pc}$.

The trigonometric parallax measured by TYCHO (TYC 9166-00716-1) is 46.5 mas. Thus, the distance would be 21.5 pc, however, this value is meaningless because LB 3459 has not been treated as a binary in the TYCHO data reduction (Wicenec priv. comm.).

3.5.1. Summary

The parameters of LB 3459 are summarized in Tab. 4. LB 3459 is He deficient by a factor of 125. C, N, O, Si are depleted by factors of about 265, 33, 12, 6, and 5, respectively. Fe and Ni are present in the photosphere at roughly solar abundances. Mg is enriched by a factor of 6. A fit of our final H+He+C+N+O+Mg+Si+Fe+Ni model to the optical observation is shown in Fig. 18. It is worthwhile to note that the slight changes in the temperature structure due to the consideration of iron-group elements (Fig. 3) results in small changes in the inner line cores only.

Table 4. Parameters of LB 3459 compared to the results of Kudritzki et al. 1982 (K 82). The solar abundance ratios are given by Holweger (1979) and Stürenburg & Holweger (1990)

Primary	this work		K 82	solar values
$T_{\rm eff}$ / kK	42.0	± 1	40.0	
$\log(g\,/\,\frac{cm}{s^2})$	5.21	± 0.1	5.3	
$n_{\rm He}\,/\,n_{\rm H}$	$8 \cdot 10^{-4}$	± 0.1 dex	$3 \cdot 10^{-3}$	$1.00 \cdot 10^{-1}$
$n_{\rm C}\,/\,n_{\rm H}$	$1.5 \cdot 10^{-6}$	± 0.3 dex		$3.98 \cdot 10^{-4}$
$n_{\rm N}\,/\,n_{\rm H}$	$3 \cdot 10^{-6}$	± 0.3 dex		$1.00 \cdot 10^{-4}$
$n_{\rm O}\,/\,n_{\rm H}$	$6.4 \cdot 10^{-5}$	± 0.5 dex		$7.94 \cdot 10^{-4}$
$n_{\rm Mg}\,/\,n_{\rm H}$	$1.9 \cdot 10^{-4}$	± 0.5 dex		$3.16 \cdot 10^{-5}$
$n_{\rm Si}\,/\,n_{\rm H}$	$8 \cdot 10^{-6}$	± 0.3 dex		$3.98 \cdot 10^{-5}$
$n_{\rm Fe}\,/\,n_{\rm H}$	$3.2 \cdot 10^{-5}$	± 0.5 dex		$3.98 \cdot 10^{-4}$
$n_{\rm Ni}\,/\,n_{\rm H}$	$3.2 \cdot 10^{-6}$	± 0.5 dex		$1.59 \cdot 10^{-6}$
$M_1\,/\,{\rm M}_\odot$	0.330	± 0.006	0.3	
$R_1\,/\,{\rm R}_\odot$	0.236	$^{+0.031}_{-0.027}$	0.18	
$L_1\,/\,{\rm L}_\odot$	170	± 6		
$v_{\rm rot}\,/\,\frac{\rm km}{\rm sec}$	34	± 10		
Secondary				
$M_2\,/\,{\rm M}_\odot$	0.066	± 0.001	0.04	
d / pc	396	$^{+50}_{-54}$	280	
$n_{\rm H}$ / cm^2	$2 \cdot 10^{20}$	$\pm 1 \cdot 10^{20}$		
$E_{\rm B-V}$	0.0526	± 0.0263	0.0	

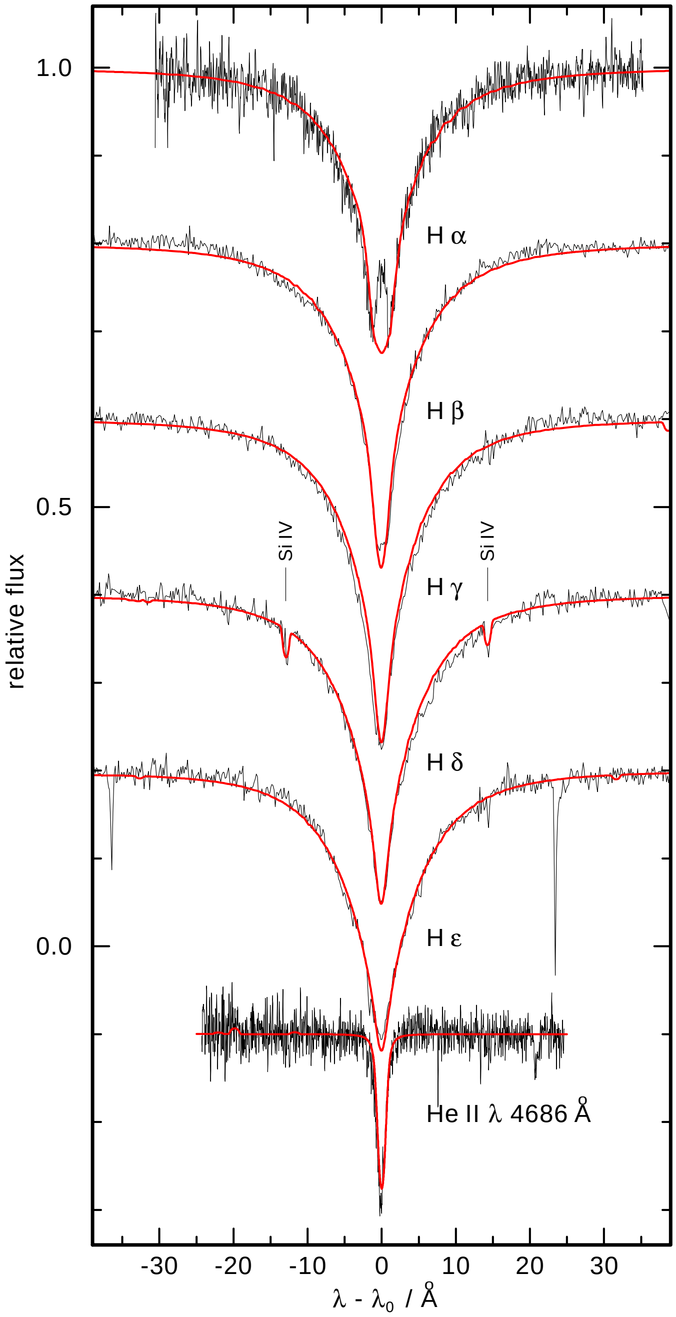

Fig. 18. Theoretical line profiles calculated from our final H+He+C+N+O+Mg+Si+Fe+Ni model, compared with the observation (Tab. 1): H α (CES), H β – H ϵ (CASPEC), He II λ 4686Å (CES). Model model parameters see Tab. 4. The emission in the line cores of H α and H β is due to the reflection from the secondary

4. Conclusions

A reliable analysis of photospheric parameters ($T_{\rm eff}$, $\log g$) requires precise element abundance determinations, even of putative trace elements, in order to model the temperature structure correctly.

In the case of LB 3459 the Balmer-line problem appears in the analysis based on pure H+He spectra. With the consideration of carbon, nitrogen, oxygen, magnesium, silicon, iron, and nickel in addition, the agreement of the theoretical Balmer lines with the observation has been improved. However, it is not perfect and there might be additional absorbers present in the photosphere which have not been considered in our analysis.

Since the ionization balance is a very sensitive indicator for $T_{\rm eff}$, the simultaneous fit of the He I and He II (Fig. 7), C III and C IV (Fig. 8), N III – N V (Fig. 9), and O IV and O V lines (Fig. 10) to the UV spectrum of LB 3459 verifies our $T_{\rm eff} = 42$kK determination (Sect. 3.2) within a small error range.

The UV spectrum of LB 3459 is full of lines of iron-group elements. Their consideration improves the fit of the synthetic spectrum to the observation. However, several features remain unidentified and may stem from "light metals" Li – Ca which are not considered in this analysis. However, from the consideration of the iron-group elements we can judge that this has only a neglectable influence on our analysis of the photospheric parameters.

The derived low helium and metal abundances (Fig. 19) indicate that diffusion is likely to be efficient in the primary of LB 3459 and responsible for the depletion. Due to the increasing number of lines with the atomic number, the radiation force and the relatively low surface gravity of LB 3459 allows the heavier elements to stay at the surface – iron and nickel appear even to be solar. Magnesium is enriched by a factor of six – no simple explanation can be given for this phenomenon. High-resolution and high-S/N UV spectra are required in order to determine the photospheric metal abundances of the primary of LB 3459 more precisely.

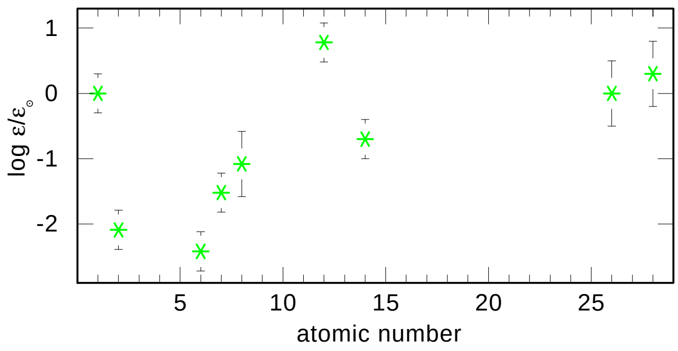

Fig. 19. Photospheric abundances of LB 3459 relative to the sun

The spectroscopically determined rotational velocity ($v_{\rm rot} = 34\pm10{\rm km}\cdot{\rm sec}^{-1}$ of the primary of LB 3459 is marginally less than $v_{\rm rot} = 45.7{\rm km}\cdot{\rm sec}^{-1}$ which can be calculated from its radius and orbital period (Sect. 1). Thus it cannot be excluded that the rotation of the primary is bound. However, new optical spectra with high S/N ratio and short exposure times are highly desirable in order to significantly improve the determination of $v_{\rm rot}$ and to minimize the influence of orbital motion on the line broadening.

Based on the assumption that the primary, subdwarf component in LB 3459 has a mass of $M_1 = 0.5\,{\rm M}_\odot$, HHH found the cool secondary star entirely consistent with ZAMS models. However, the newly determined, low masses of the primary ($M_1 = 0.330\,{\rm M}_\odot$) and secondary ($M_2 = 0.066\,{\rm M}_\odot$) component of LB 3459 suggest that this is a "low mass case B" system (Iben & Livio 1993). Thus, it appears possible that the secondary has formerly been a planet ($M_2 < 0.05\,{\rm M}_\odot$) which has survived the CE phase ($M_2 > M_{\rm crit} \approx 0.02\,{\rm M}_\odot$) and even has gained mass.

The uncertainties in the evolutionary scenario of LB 3459 may be a reason for the disagreement with the results from light curve and velocity curve analyses. Although the character of the primary appears clear, almost nothing is known about the secondary. Moreover, the experienced CE phase questions the validity of the evolutionary models of Driebe et al. (1998) for LB 3459 – although these are the most elaborated for similar, non-CE stars.

Acknowledgements. We like to thank Horst Drechsel, Uli Heber, and Klaus Werner for helpful discussions and Jochen L. Deetjen for assistance with calculation of the iron-group cross sections. This research was supported by the DLR under grant 50 OR 9705 5. Computations were carried out on CRAY computers of the Rechenzentrum der Universität Kiel. This research has made use of the SIMBAD Astronomical Database, operated at CDS, Strasbourg, France, and of the NIST atomic spectra database.

References

Bevington P.R., Robinson D.K. 1992, Data reduction and error analysis for the physical sciences, McGraw-Hill Inc., New York

Deetjen J.L., Dreizler S., Rauch T., Werner K. 1999, A&A 348, 940

Dreizler S., Werner K. 1994, A&A 286, L 31

Driebe T., Schönberner D., Blöcker T., Herwig F. 1998, A&A 339, 129

Feast M.W., Thackeray A.D., Wesselink A.J. 1960, MNRAS 121, 25

Groenewegen M.A.T., Lamers H.J.G.L.M. 1989, A&AS 79, 359

Heber U., Hunger K., Jonas G., Kudritzki R.P. 1984, A&A 130, 119

Heber U., Hunger K., Rauch T., Werner K 1988, in: Proc. IAU Symposium 132, G. Cayrel de Strobel, M. Spite (eds.), Kluwer, Dordrecht, p. 117

Hilditch R.W., Harries T.J., Hill G. 1996, MNRAS 279, 1380

Holweger H. 1979, Les Elements et leurs Isotopes dans l'Univers, Universite de Liège, Inst. d. Astrophysique, p. 117

Hubeny I., Hummer D.G., Lanz T. 1994, A&A 282, 157

Hummer D.G., Mihalas D. 1988, ApJ 331, 794

Iben I.Jr., Livio M. 1993, PASP 105, 1373

Kilkenny D., Hilditch R.W., Penfold J.E. 1978, MNRAS 183, 523

Kilkenny D., Penfold J.E., Hilditch R.W. 1979, MNRAS 187, 1

Kilkenny D., Hill P.W., Penfold J.E. 1981, MNRAS 194, 429

de Kool M., Ritter H. 1993, A&A 267, 397

Kudritzki R.P. 1976, A&A 52, 11

Kudritzki R.P., Simon K.P., Lynas-Gray A.E., Kilkenny D., Hill P.W. 1982, A&A 106, 254

Lemke M. 1997, A&AS 122, 285

Lynas-Gray A.E., Heber U., Kudritzki R.P., Simon K.P. 1984, in: Proc. 4th European IUE Conference, Rome, ESA SP-218, p. 285

Napiwotzki R., Rauch T. 1994, A&A 285, 60

Paczynski B. 1980, Acta Astr. 34, 381

Press W.H., Teukolsky S.A., Vetterling W.T., Flannery B.P. 1992, Numerical Recipes, 2nd ed., Cambridge University Press

Rauch T., 1987, diploma thesis, University Kiel

Rauch T., 1997, A&A 320, 237

Schöning T., Butler K. 1989, A&AS 78, 51

Stürenburg S., Holweger H. 1990, A&A 237, 125

Vidal C.R., Cooper J., Smith E.W. 1973, ApJS 25, 37

Werner K. 1988, A&A 204, 159

Werner K. 1996, ApJ 457, L39

Werner K., Husfeld D. 1985, A&A 148, 417

Wesselink A.J. 1962, MNRAS 124, 359